Molecular Recognition of Methylated Amino Acids and Peptides by Pillar[6]MaxQ

Journal Name

FULL PAPER

Molecular Recognition of Methylated Amino Acids and Peptides by Pillar[6]MaxQ

David King,[a] Chelsea R. Wilson,[b] Lukas Herron,[c,d] Chun-Lin-Deng,[a] Shams Mehdi,[c,d] Pratyush Tiwary,[a,d,*] Fraser Hof,[b,*] and Lyle Isaacs[a,*]

We report the molecular recognition properties of Pillar[n]MQ (P[n]MQ) toward a series of (methylated) amino acids, amino acid amides, and post-translationally modified peptides by a combination of ^{1}H NMR, isothermal titration calorimetry, indicator displacement assays, and molecular dynamics simulations. We find that P6MQ is a potent receptor for N-methylated amino acid side chains. P6MQ recognized the H3K4Me$_3$ peptide with K_d = 16 nM in phosphate buffered saline.

Introduction

The design and realization of advanced supramolecular systems for a variety of biological (e.g. drug delivery, *in vivo* imaging, sequestration) and chemical (sensing, purifications, catalysis) applications is accelerated by the ready availability of a diverse set of building blocks. Molecular containers – cyclodextrins, calix[n]arenes, crown ethers, cyclophanes, coordination cages, molecular clips and tweezers, cucurbit[n]urils (CB[n]), H-bonded capsules, pillararenes, and others – are among the most commonly employed building blocks.[1] When considering biosupramolecular applications, good water solubility, excellent biocompatibility, and high binding affinity in salty water are particularly important.[2] Over the past decade, the synthesis, molecular recognition properties, and applications (e.g. drug delivery, fluorescent materials, chemical sensing, supramolecular antidotes, supramolecular catalysis, and porous materials) of organic and water soluble pillar[n]arenes has developed rapidly and been thoroughly reviewed.[3] WPn (Figure 1) which feature CH$_2$CO$_2$Na solubilizing groups, good

biocompatibility and good host•guest binding affinity are particularly popular and have been used to recognize lysine and arginine[4,5]. Recently, we reported that Pillar[n]MaxQ (P[n]MQ) which feature OSO$_3$Na groups displayed greatly enhanced binding affinity compared to WPn, especially toward tertiary and quaternary ammonium ions.[6]
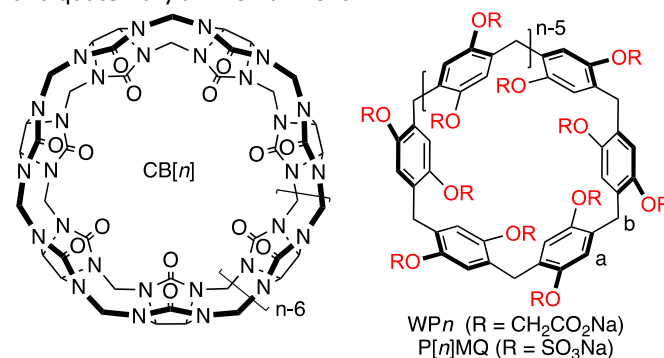

Figure 1 Chemical structures of CB[n] and pillararene receptors.

As a new host the biosupramolecular applications of P[n]MQ have not been explored. One important application of cation receptors like P[n]MQ is the binding and detection of biomarkers. Post-translational modifications (PTMs) play an important role in the regulation of protein function.[7] The N-methylation of lysine and arginine on the tail of histone 3 (H3) is an important class of PTMs. These methylation signatures have the potential to act as biomarkers in various diseases.[8] For example, high levels of H3K4 trimethylation (H3K4Me$_3$) have been associated with a poor patient outcome in hepatocellular carcinoma.[9] These methylations commonly occur inside the nucleus where methyl transferase and demethylase enzymes orchestrate the degree of methylation resulting in distinct chromatin structure, function, and ultimately biological outcome.[10] To study the methylated states of lysine and arginine, chemical tools are needed that can selectively recognize the methylated over non-methylated residue. Accordingly, the molecular recognition of post-translationally methylated amino acid residues has been investigated using a

a. *Department of Chemistry and Biochemistry, University of Maryland, College Park, Maryland 20742, USA. E-mail: lisaacs@umd.edu.*
b. *Department of Chemistry, University of Victoria, Victoria, BC, V8W 3V6, Canada. Email: fhof@uvic.ca*
c. *Biophysics Program, University of Maryland, College Park, MD 20742, United States.*
d. *Institute for Physical Science and Technology, University of Maryland, College Park, MD 20742, United States. Email: ptiwary@umd.edu*

variety of supramolecular hosts as a route toward new diagnostics and therapeutics.[11] Given our collective interest in using molecular containers in biosupramolecular applications[12] and the observed high selectivity of P6MQ for tertiary and quaternary ammonium ions,[6] we decided to explore the molecular recognition properties of P[n]MQ toward methylated vs. non-methylated amino acids, amino acid amides, and the methylated peptide fragments of the histone 3 tail.

Results and Discussion

This results and discussion section is organized as follows. First, we present the measurement of the binding affinity of P5MQ and P6MQ toward a series of (methylated) amino acids and amino acid amides by isothermal titration calorimetry and discuss trends in the data. Subsequently, we present investigations of the geometry of the stronger host•guest complexes by ^{1}H NMR spectroscopy. Given the high binding affinity of P6MQ toward methylated amino acids, we next used indicator displacement assays to measure the binding of P6MQ toward a series of post-translationally modified peptides

derived from the tail of histone 3. Finally, we present the results of all-atom explicit water[13] molecular dynamics (MD) simulations to gain insight into the geometrical features and the driving forces for the P6MQ complexation events.

Selection of Amino Acids and Amino Acid Amides. As described above, we have previously studied the binding of P[n]MQ toward a series of cationic and dicationic guests that also differ in the degree of alkylation of the cationic N-atoms.[6] We observed that P[n]MQ preferentially binds to quaternary over primary diammonium ions and that monocations bind more weakly than dications.[6] Accordingly, we selected a series of amino acids, amino acid amides, and N-acetyl amino acid amides (Figure 2) that allow us to assess the importance of: 1) ion-ion interactions (e.g. H-K-OH vs. H-K-NH$_2$ vs. Ac-K-NH$_2$), 2) the degree of methylation of the cationic side chains on lysine and arginine, and 3) the nature of the hydrophobic residue on the complexation strength.
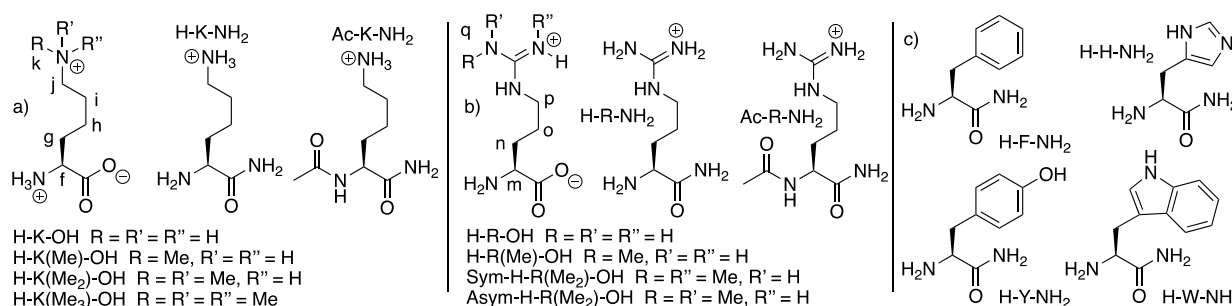

Figure 2 Chemical structures of: a) lysine derivatives, b) arginine derivative, and c) other amino acids used in this study.
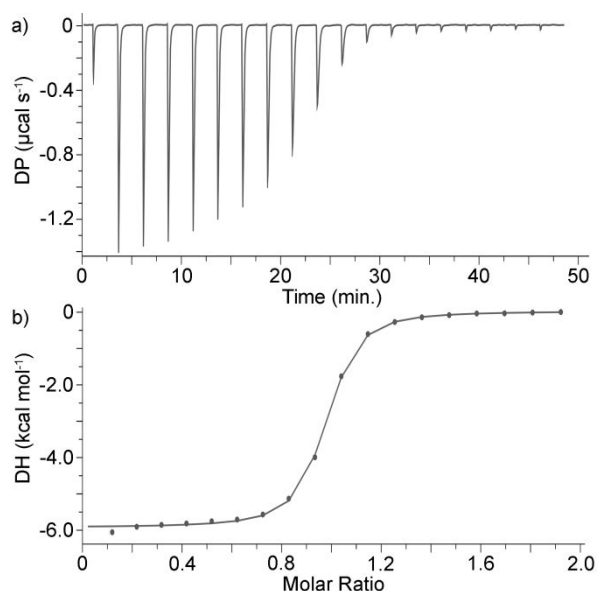

Figure 3 a) ITC thermogram recorded during the titration of P6MQ (100 μM) in the cell with H-K(Me$_3$)-OH (1.0 mM) in the syringe. b) Fitting of the data to a 1:1 binding model with K_a = (3.39 ± 0.15) × 10^6 M^{-1}. Conditions: phosphate buffered saline, pH 7.4, 298.0 K.

Measurement of Thermodynamic Parameters by Isothermal Titration Calorimetry (ITC). We first decided to measure the

thermodynamic parameters of complexation for P[n]MQ with the panel of amino acid derivatives shown in Figure 2. Given the known ultratight binding of P[n]MQ toward cationic guests,[6] we expected that the strength of some of the P[n]MQ•amino acid complexes would exceed the range that is measured accurately by ^{1}H NMR titrations (K_a > 10^4 M^{-1}).[14] Accordingly, we elected to use ITC as the main analytical technique. Figure 3a shows the thermogram recorded when a solution of P6MQ (0.1 mM) in the cell was titrated with a solution of H-K(Me$_3$)-OH (1.0 mM) from the syringe. Integration of the data in Figure 3a allows the construction of a plot of ΔH versus molar ratio (Figure 3b) which was fitted to a standard 1:1 binding isotherm using the PEAQ data analysis software to extract K_a = (3.39 ± 0.15) × 10^6 M^{-1} and ΔH = -5.94 ± 0.02 kcal mol^{-1}. The results of related direct titrations of P5MQ and P6MQ with the panel of amino acid derivatives (Figure 2) were performed similarly and the results are collected in Table 1. For the weaker complexes (e.g. K_a < 10^4 M^{-1}), the working concentrations of host and the guest were increased in order sample a larger portion of the binding isotherm (e.g. more appropriate ITC c-value.[15] The binding constants for the P5MQ•guest complexes span from 926 M^{-1} to 5.42 x 10^5 M^{-1} whereas those of P6MQ•guest span from 1740 M^{-1} to 3.20 x 10^6 M^{-1}. All of the complexes are driven by favorable changes in enthalpy (ΔH) upon complexation. This thermodynamic signature is well known for macrocyclic hosts

           FULL PAPER

(e.g. cyclodextrins, cyclophanes, CB[*n*], pillararenes) where it is known as the non-classical hydrophobic effect which is due to the release of water molecules from the cavity of uncomplexed host•guest complexation.[16]

Table 1 Thermodynamic parameters (K_a [M^{-1}], $\Delta H°$ [kcal mol^{-1}]) determined for the P5MQ•guest and P6MQ•guest complexes by ITC. Conditions: 298K, PBS buffered H$_2$O, pH 7.4.

	P5MQ		P6MQ	
Guest	K_a (M^{-1})	ΔH (kcal mol^{-1})	K_a (M^{-1})	ΔH (kcal mol^{-1})
H-R-OH	$(3.77 \pm 0.24) \times 10^3$	-6.57 ± 0.18	$(5.85 \pm 0.13) \times 10^3$	-6.65 ± 0.06
H-R(Me)-OH	$(5.87 \pm 0.17) \times 10^3$	-5.50 ± 0.19	$(1.15 \pm 0.04) \times 10^4$	-5.42 ± 0.05
Sym-H-R(Me$_2$)-OH	$(5.35 \pm 0.16) \times 10^3$	-4.84 ± 0.05	$(6.45 \pm 0.36) \times 10^4$	-4.78 ± 0.10
Asym-H-R(Me$_2$)-OH	$(3.25 \pm 0.34) \times 10^3$	-3.36 ± 0.16	$(1.71 \pm 0.06) \times 10^5$	-6.64 ± 0.12
H-R-NH$_2$	$(2.12 \pm 0.06) \times 10^5$	-8.01 ± 0.13	$(1.16 \pm 0.03) \times 10^6$	-11.2 ± 0.0
Ac-R-NH$_2$	$(3.27 \pm 0.29) \times 10^4$	-4.94 ± 0.30	$(4.51 \pm 0.17) \times 10^4$	-8.49 ± 0.11
H-K-OH	$(9.26 \pm 2.67) \times 10^2$	-1.70 ± 0.38	$(1.74 \pm 0.09) \times 10^3$	-4.84 ± 0.14
H-K(Me)-OH	$(1.24 \pm 0.23) \times 10^3$	-4.79 ± 0.61	$(9.19 \pm 0.18) \times 10^3$	-5.13 ± 0.03
H-K(Me$_2$)-OH	$(6.13 \pm 0.18) \times 10^3$	-7.31 ± 0.20	$(2.52 \pm 0.05) \times 10^5$	-8.10 ± 0.04
H-K(Me$_3$)-OH	$(1.76 \pm 0.07) \times 10^4$	-10.8 ± 0.3	$(2.89 \pm 0.13) \times 10^6$	-6.44 ± 0.02
H-K-NH$_2$	$(5.42 \pm 0.10) \times 10^5$	-9.67 ± 0.11	$(3.20 \pm 0.19) \times 10^6$	-10.5 ± 0.0
Ac-K-NH$_2$	$(7.19 \pm 0.28) \times 10^4$	-7.99 ± 0.20	$(9.29 \pm 0.46) \times 10^4$	-9.37 ± 0.11
H-H-NH$_2$	n.b.	n.b.	$(9.01 \pm 2.49) \times 10^3$	-6.09 ± 0.04
H-F-NH$_2$	n.b.	n.b.	$(4.43 \pm 0.25) \times 10^4$	-9.54 ± 0.03
Ac-F-NH$_2$	–	–	$(5.99 \pm 1.89) \times 10^4$	-2.39 ± 0.03
H-Y-NH$_2$	n.b.	n.b.	$(2.66 \pm 0.30) \times 10^4$	-12.0 ± 0.2
H-W-NH$_2$	n.b.	n.b.	$(8.20 \pm 1.28) \times 10^3$	-7.62 ± 0.02

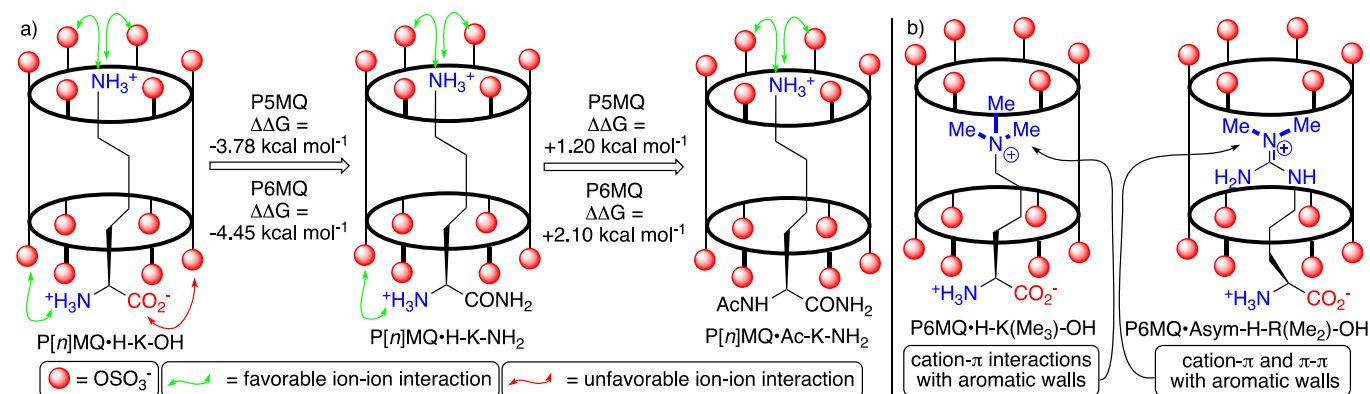n.b. = no heat detected. – = not measured.

Figure 4 a) Cartoon of the interaction of P[*n*]MQ with lysine, lysine amide, and N-Acetyl-lysine amide. The green and red double headed arrows spotlight favorable and unfavorable electrostatic interactions, respectively. b) Illustration of the proposed geometries of the P6MQ•H-K(Me$_3$)-OH and P6MQ•Asym-H-R(Me$_2$)-OH complexes.

Influence of Ion-Ion Interactions on the Molecular Recognition of P[n]MQ Toward Amino Acids and Amino Acid Amides. The data in Table 1 allows us to discern the influence of ion-ion interactions on the binding of the poly-anionic P5MQ and P6MQ hosts toward ionic guests. For example, lysine (H-K-OH) and arginine (H-R-OH) are expected to be overall cationic at neutral pH although they contain two cationic and one anionic group. Figure 4a shows a cartoons of the proposed geometry P[*n*]MQ•H-K-OH derivative complexes and highlights the attractive NH$_3$$^+$•••$^-O_3$SO and repulsive CO$_2$$^-$•••$^-O_3$SO ion-ion interactions. In contrast, lysine amide (H-K-NH$_2$) and arginine amide (H-R-NH$_2$) are dicationic at neutral pH and do not suffer the unfavorable CO$_2$$^-$•••$^-O_3$SO interactions. Conversely N-acetyl-lysine amide (Ac-K-NH$_2$) and N-Acetyl-arginine amide (Ac-R-NH$_2$) are mono-cationic at neutral pH and should benefit from favorable NH$_3$$^+$•••$^-O_3$SO interactions. Figure 4a shows the differences in binding free energy of the P[*n*]MQ•H-K-OH versus the P[*n*]MQ•H-K-NH$_2$ complexes and the P[*n*]MQ•H-K-NH$_2$ versus P[*n*]MQ•Ac-K-NH$_2$ complexes. The elimination of the unfavorable CO$_2$$^-$•••$^-O_3$SO interactions results in complexes that are substantially more stable (P5MQ: $\Delta\Delta G$ = -3.78 kcal mol^{-1}; P6MQ: $\Delta\Delta G$ = -4.45 kcal mol^{-1}) whereas the elimination of favorable NH$_3$$^+$•••$^-O_3$SO interactions is energetically costly (P5MQ: $\Delta\Delta G$ = +1.20 kcal mol^{-1}; P6MQ: $\Delta\Delta G$ = +2.10 kcal mol^{-1}).

Values for the P[n]MQ•H-R-OH to P[n]MQ•H-R-NH$_2$ (P5MQ: $\Delta\Delta G$ = -2.38 kcal mol^{-1}; P6MQ: $\Delta\Delta G$ = -3.13 kcal mol^{-1}) and P[n]MQ•H-R-NH2 to P[n]MQ•Ac-R-NH$_2$ (P5MQ: $\Delta\Delta G$ = +1.46 kcal mol^{-1}; P6MQ: $\Delta\Delta G$ = +1.92 kcal mol^{-1}) complexes show similar trends for similar pairwise comparisons. We conclude that favorable electrostatic interactions (cation•••anion) provide an important driving force for P[n]MQ•amino acid derivative complexation and that unfavorable (anion•••anion) electrostatic interactions can result in large free energy penalties.

Influence of the Degree of Methylation on the Molecular Recognition of P[n]MQ Toward Amino Acids and Amino Acid Amides. The panel of amino acid derivatives contains a series of lysine (H-K-OH, H-K(Me)-OH, H-K(Me$_2$)-OH, H-K(Me$_3$)-OH) and arginine (H-R-OH, H-R(Me)-OH, Sym-H-R(Me$_2$)-OH, Asym-H-R(Me$_2$)-OH) derivatives that differ in the degree and pattern of methylation. As the degree of methylation increases across the series of lysine derivatives, we observe that K_a values toward P5MQ and P6MQ increases 19-fold and 166-fold, respectively (Table 1). Similarly, along the series of methylated arginine derivatives, we observe a 29-fold increase in binding affinity for P6MQ•Asym-H-R(Me$_2$)-OH compared to P6MQ•H-R-OH. The increased affinity of P6MQ toward the more highly methylated amino acid derivatives is consistent with the previously reported binding of P[n]MQ toward alkane diammonium ions,[6] and also with other macrocyclic host systems. We believe that the more hydrophobic NMe$_3^+$ group enhances both the hydrophobic effect and the cation-π components of binding which allows the P6MQ•H-K(Me$_3$)-OH complex to assume the geometry shown in Figure 4, and which in turn reduces the unfavorable electrostatic interactions (CO$_2^-$•••$^-$O$_3$SO) upon binding.

Influence of the Nature of the Hydrophobic Residue on Binding. The P6MQ host features two equivalent hexa-anionic portals separated by a hydrophobic cavity which explains the tight binding exhibited toward derivatives of lysine and arginine which feature hydrophobic and cationic sidechains. To gain insight into the importance of the nature of the hydrophobic side chain, we determined the binding between P[n]MQ and the four aromatic amino acid amides (H-H-NH$_2$, H-F-NH$_2$, H-Y-NH$_2$, H-W-NH$_2$) which feature imidazole, phenyl, hydroxyphenyl, and indole rings (Table 1). We find that all four P6MQ•aromatic amino acid amide K_a values cluster in the range of 8200 – 44300 M^{-1}. In contrast, no heat was detected during the titration of P5MQ (100 μM) with the four amino acid amides which is indicative of weak binding (K$_a$ < 10^4 M^{-1}). This weak binding of these aromatic amino acid derivatives arise due to the narrower cavity of P5MQ which recognized linear alkyl chains preferentially over aromatic rings. Related ITC titrations of P6MQ and methionine amide, leucine amide, or glutamine amide did not show any heat evolved indicating even weaker binding for these amino acid amides. Taken together, these results suggest that the presence of an aromatic side chain promotes complexation by $\pi-\pi$ interactions with the walls of P6MQ, but that the presence of a cationic and preferably

methylated sidechain (e.g. lysine or arginine) is needed to achieve submicromolar binding in PBS buffered water.
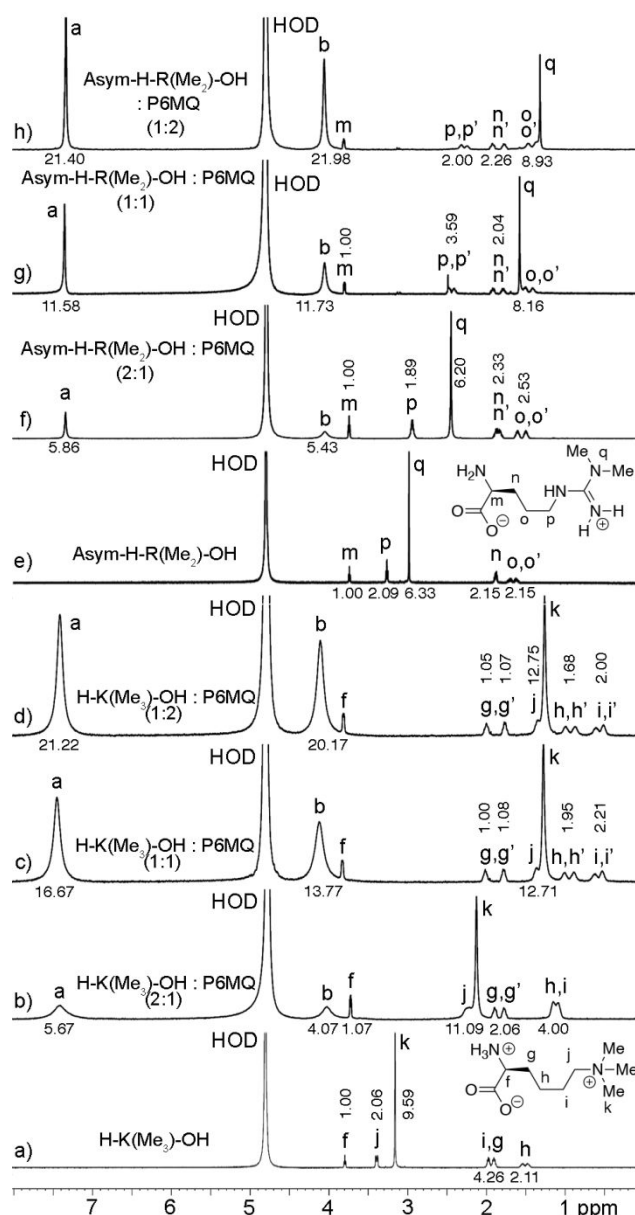

Figure 5 ^{1}H NMR spectra recorded (600 MHz, RT, 20 mM phosphate buffered D$_2$O, pH 7.4) for: a) H-K(Me$_3$)-OH (1.0 mM), b) a mixture of H-K(Me$_3$)-OH (1.0 mM) and P6MQ (0.5 mM), c) a mixture of H-K(Me$_3$)-OH (1.0 mM) and P6MQ (1.0 mM), d) a mixture of H-K(Me$_3$)-OH (1.0 mM) and P6MQ (2.0 mM), e) Asym-H-R(Me$_2$)-OH (1 mM), f) a mixture of Asym-H-R(Me$_2$)-OH (1 mM) and P6MQ (0.5 mM), g) a mixture of Asym-H-R(Me$_2$)-OH (1.0 mM) and P6MQ (1.0 mM), and h) a mixture of Asym-H-R(Me$_2$)-OH (1.0 mM) and P6MQ (2.0 mM).

Qualitative ^{1}H NMR Host•Guest Recognition Study. Having determined the thermodynamic parameters of binding, we proceeded to glean information on the geometry of the tighter host guest complexes (P6MQ•Asym-H-R(Me$_2$)-OH and P6MQ•H-K(Me$_3$)-OH) by ^{1}H NMR spectroscopy. Figure 5a shows the ^{1}H NMR recorded for H-K(Me$_3$)-OH in PBS using the labelling scheme given in Figures 1 and 2. Figure 5c shows the ^{1}H NMR spectrum of an equimolar mixture of P6MQ and H-K(Me$_3$)-OH.

We observe that the methonium group (H$_k$; $\Delta\delta$ = -1.9 ppm) and the methylene groups alpha (H$_j$; $\Delta\delta$ = -2.0 ppm) and beta (H$_i$; $\Delta\delta$ = -1.4 ppm) to NMe$_3^+$ undergo substantial upfield shifts upon formation of P6MQ•H-K(Me$_3$)-O*H* whereas the protons closer to the carboxylate substituent (e.g. H$_f$, H$_g$, H$_h$) undergo small to no change in chemical shift upon binding. This pattern of changes in chemical shift establishes that the Me$_3$NCH$_2$CH$_2$ group is located within the anisotropic magnetic shielding environment of the P6MQ cavity whereas the carboxylate terminus is located outside the cavity. The resonances for H$_a$ and H$_b$ of P6MQ do not undergo significant ($\Delta\delta \leq$ 0.1 ppm) changes in chemical shift upon complexation. The proposed geometry of P6MQ•H-K(Me$_3$)-OH is presented in Figure 4b. This geometry allows for maximization of the cation-π and CH-π interactions between the electrostatically positive Me$_3$N$^+$CH$_2$ group and the electron rich aromatic walls of the cavity. Figure 5b shows the ^{1}H NMR spectrum of a 1:2 mixture of P6MQ and

H-K(Me$_3$)-OH; the presence of a single set of resonances for H-K(Me$_3$)-OH at chemical shifts in between those of uncomplexed H-K(Me$_3$)-OH and P6MQ•H-K(Me$_3$)-OH establishes fast kinetics of exchange on the chemical shift timescale. Figure 5e-h shows a similar set of ^{1}H NMR spectra recorded for for Asym-H-R(Me$_2$)-OH. Formation of the P6MQ•Asym-H-R(Me$_2$)-OH complex results in substantial upfield shifts for methylated guanidinium group (H$_q$, $\Delta\delta$ = -1.7 ppm; H$_p$, $\Delta\delta$ = -1.0 ppm) and only small shifts for the protons closer to the carboxylate group (H$_m$, $\Delta\delta$ = +0.1 ppm; H$_n$, $\Delta\delta \leq$ 0.1 ppm; H$_o$, $\Delta\delta$ = -0.15 ppm). The direction and magnitude of the changes in chemical shift upon formation of the P6MQ•Asym-H-R(Me$_2$)-OH complex indicated that the dimethyl arginine unit is bound within the magnetic shielding environment of the P6MQ cavity where it benefits from cation-π and $\pi-\pi$ interactions with the walls of the P6MQ host as illustrated in Figure 4b.
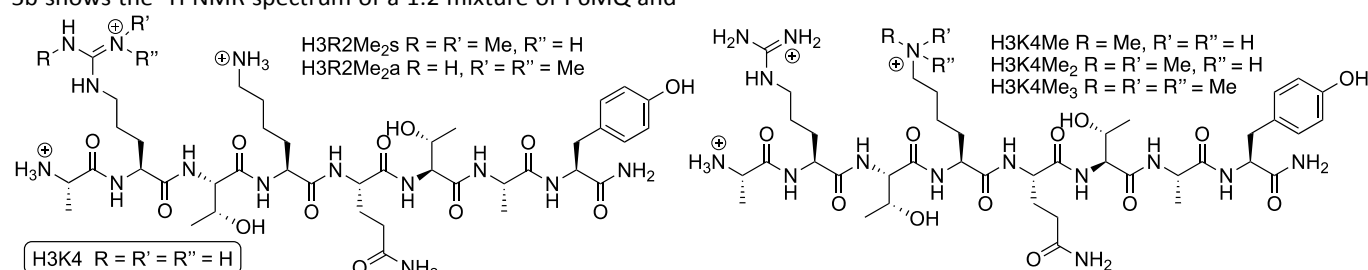

Figure 6 Structure of the histone H3K4 peptides used in this study.
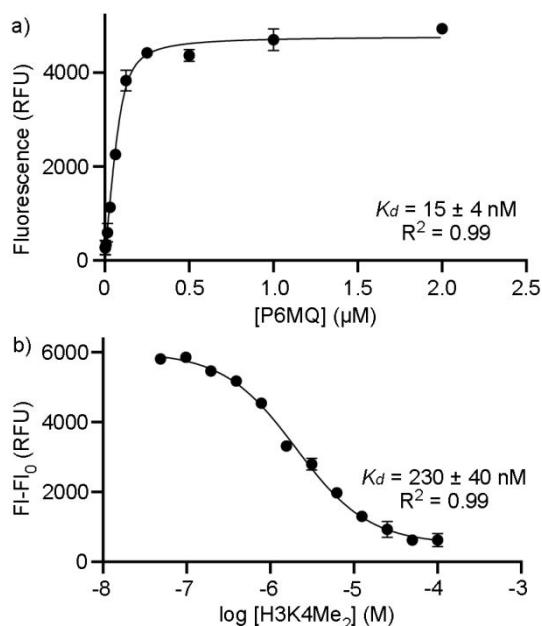

Figure 7 a) Direct fluorescence titration of a solution of DAPI (100 nM) with a solution of P6MQ in phosphate buffered saline at pH 7.4. b) Competitive fluorescence titration of a solution of P[6]AS (125 nM) and DAPI (100 nM) with a solution of H3K4Me$_2$ in phosphate buffered saline at pH 7.4. Reported dissociation constants are the average of six measurements, curves and R^2 of exemplary triplicate data (see Supporting Information).

Molecular Recognition of H3K4 Peptides by P6MQ Monitored by Fluorescence Titrations. The high binding affinities of P6MQ toward H-R-NH$_2$, H-K(Me$_3$)-OH, Asym-H-R(Me$_2$)-OH and Sym-H-R(Me$_2$)-OH prompted us to study the interaction of P6MQ

towards a peptide fragment of the histone 3 (which will be referred to as H3K4) and the various *N*-methylated states of arginine at position 2 (R2) or lysine at position 4 (K4) (Figure 6). Given the high binding constants observed (*vide infra*) and the small quantities of the peptides available, we decided to use direct and competitive fluorescence titrations to measure the binding constants for the P6MQ•peptide complexes. Through the screening of various host:dye complexes we found 4′,6-diamidino-2-phenylindole (DAPI) was a suitable fluorescent guest for indicator displacement assay. DAPI is well known to bind to AT-rich regions of DNA and undergo an ≈ 20-fold enhancement of fluorescence;[17] DAPI also binds to other macrocyclic cation receptors (e.g. CB[7]).[18] First, we performed a direct titration of a solution of DAPI (100 nM) with a solution of P6MQ (0 – 2 μM) and monitored the emission at 450 nm after excitation at 360 nm. Figure 7a shows a plot of fluorescence (RFU) versus concentration fitted to a standard 1:1 host:guest binding model (Supporting Information) which allowed the determination of K_d = 15 ± 4 nM for P6MQ•DAPI in PBS. Subsequently, we implemented an indicator displacement assay[19] using DAPI as a fluorescent indicator to determine the binding of P6MQ toward the H3 peptides. For this purpose, we titrated a solution of P6MQ (125 nM) and DAPI (100 nM) with a solution of H3 peptide and monitored the fluorescence emission at 450 nm. Figure 7b shows a plot of change in fluorescence versus [H3K4Me$_2$] fitted to a competitive binding model which allows for the determination of K_d = 230 ± 40 nM for the P6MQ•H3K4Me$_2$ complex. The binding constants for the remaining P6MQ•H3 peptide complexes were measured analogously and the results are presented in Table 2.

Interestingly, we find that H3K4, H3K4Me, and H3K4Me$_2$ bind with sub-micromolar affinity to P6MQ by factors of >1000, >300, and 17-fold stronger than the corresponding amino acids H-K-OH, H-K(Me)-OH, and H-K(Me$_2$)-OH, respectively. This enhancement of affinity can be rationalized by the removal of the unfavorable anion-anion interactions (CO$_2^-$•••$^-$O$_3$SO, Figure 4) and by the additional cationic residues on the guest (N-terminus and side chain residue). The H3K4Me$_3$ peptide is the strongest binder in the series (P6MQ•H3K4Me$_3$, K_d = 16 nM) and binds 14-fold stronger than the unmodified peptide as expected based on the preference of P6MQ for quaternary ammoniums.[6] The nanomolar affinity of P6MQ towards the known biomarker H3K4Me$_3$ in a salty media (137 mM NaCl) indicates the potential of P6MQ to be used in biological systems. To our knowledge P6MQ has the strongest reported affinity to H3K4Me$_3$ of any supramolecular host. Additionally, the H3R2Me$_2$a and H3R2Me$_2$s peptides also bind P6MQ with K_d values of 50 nM and 70 nM, respectively. These binding constants are 117-fold and 221-fold stronger than for the analogous amino acid complexes P6MQ•Asym-H-R-OH and P6MQ•Sym-H-R-OH which again shows the loss of unfavorable CO$_2^-$•••$^-$O$_3$SO interactions. Encouraged by the high levels of binding affinity and good selectivity for the methylated H3 peptides, we decided to delve into the complexation geometries and driving forces computationally.

Table 2 P6MQ•peptide dissociation constants (K_d, nM) measured by fluorescence detected indicator displacement assays. Conditions: 10 mM PBS buffered H$_2$O, pH 7.4.

Guest	K_d (nM)
H-K(Me$_3$)-OH	430 ± 70
H3K4	540 ± 70
H3K4Me	340 ± 50
H3K4Me$_2$	230 ± 40
H3K4Me$_3$	16 ± 3
H3R2Me$_2$a	50 ± 6
H3R2Me$_2$s	70 ± 10

Investigation of the Binding Processes of P6MQ Toward Amino Acids, Amino Acid Amides, and H3 Peptides by Molecular Dynamics Simulations. The high binding affinities of P6MQ toward H-R-NH$_2$, H-K(Me$_3$)-OH and especially the H3 peptides prompted us to perform molecular dynamics simulations to better understand the geometry and the molecular determinants behind the complexation driving forces. A total of eight systems were studied: uncomplexed P6MQ, P6MQ•H-K-OH, P6MQ•H-K-NH$_2$, P6MQ•H-K(Me$_3$)-OH, P6MQ•H3K4 (lysine bound), P6MQ•H3K4 (arginine bound), P6MQ•H3K4Me$_3$ (KMe$_3$ bound), and P6MQ•H3K4Me$_3$ (arginine bound). All the systems were initialized in a physically reasonable configuration, using Spartan for the H3 complexes.[20] The complexes were parameterized using the AMBER GAFF2 force field and each system was neutralized with Na$^+$ and Cl$^-$ counter-ions at a concentration of 0.15 M to reflect the nature of the PBS buffer

used experimentally.[21] The equilibration and production simulations used the Nose-Hoover thermostat[22] and the Parrinello-Rahman barostat[23] held at 298 K and 1 bar, placing the simulation under the constant number, pressure, and temperature (NPT) ensemble. In all cases the GROMACS[24] simulation engine was used to perform the equilibration and production simulations, and calculations were performed using PLUMED.[25] Below, we separately report our observations derived from these MD simulations separately for uncomplexed P6MQ, P6MQ•amino acid (amide), and P6MQ•H3 peptide complexes.

Uncomplexed P6MQ. The (in)ability of water to solvate the hydrophobic cavity of uncomplexed macrocyclic hosts has been shown to provide an important enthalpic driving force for high affinity hosts.[16] Accordingly, we performed MD simulation of uncomplexed P6MQ to explore its aqueous solvation. We analyzed the number of hydrogen bonds (n_{HB}) that each water molecule participates in within a distance r of the center of mass of P6MQ using equation 1 where the function Hbonds(X,Y) counts the number of hydrogen bonds formed between the groups X and Y. In Eq. 1 P6MQ and LIG represent the hydrogen bond acceptors and donors atoms of the host and bound ligand which accept and donate hydrogen bonds (N, O, H), and H$_2$O$_{int}$ and H$_2$O$_{ext}$ respectively refer to water molecules within and outside of the region of interest defined by r. For uncomplexed P6MQ, no ligand is considered (*vide infra* for liganded systems).

$$n_{HB}(r) = 2 \times \text{Hbonds}(H_2O_{int}, H_2O_{int}) + \text{Hbonds}(H_2O_{int}, H_2O_{ext}) + \text{Hbonds}(H_2O_{int}, P[6]AS) + \text{Hbonds}(H_2O_{int}, LIG) \quad (1)$$

Figure 8a shows a free energy plot of the number of hydrogen bonds formed within 6 Å of the P6MQ center of mass for bulk water, P6MQ, and various P6MQ•ligand complexes. We find that the number of hydrogen bonds formed per water within 6 Å of the center of mass of uncomplexed P6MQ (1.93) is substantially smaller than the number formed per water in bulk water (3.5). The H-bond deficiency of waters encapsulated inside other hosts have been tabulated previously Biedermann, Nau, and Schneider and range from 1.00 for Klaerner's tweezer to 3.06 for CB[8].[16d] What disrupts the H-bonding network for P6MQ? We find that waters between 4Å and 6Å from the center of mass of P6MQ (e.g. near the portals) tend to form H-bonds to the sulfate groups of P6MQ, orienting the O-H bonds outward and pointing the O-atoms inwards with a deficiency of H-Bonds. In contrast, for H$_2$O molecules in the core of the P6MQ cavity (r < 4Å), we find two distinct populations of water depending on whether a Na$^+$ ion is present in the core of the P6MQ cavity. In the presence of Na$^+$ ions (Figure 8b,c), water molecules orient themselves such that the O-atoms coordinate to the Na$^+$ ion at the center of the P6MQ cavity resulting in large deficiency of H-bonds. In the relatively rare event that an Na$^+$ ion is not present inside P6MQ, 2.15 H-bonds are formed on average between H$_2$O molecules and different H-bond topologies arise due to the confinement inside P6MQ. For example, a cyclic H-bonding network comprising five or six

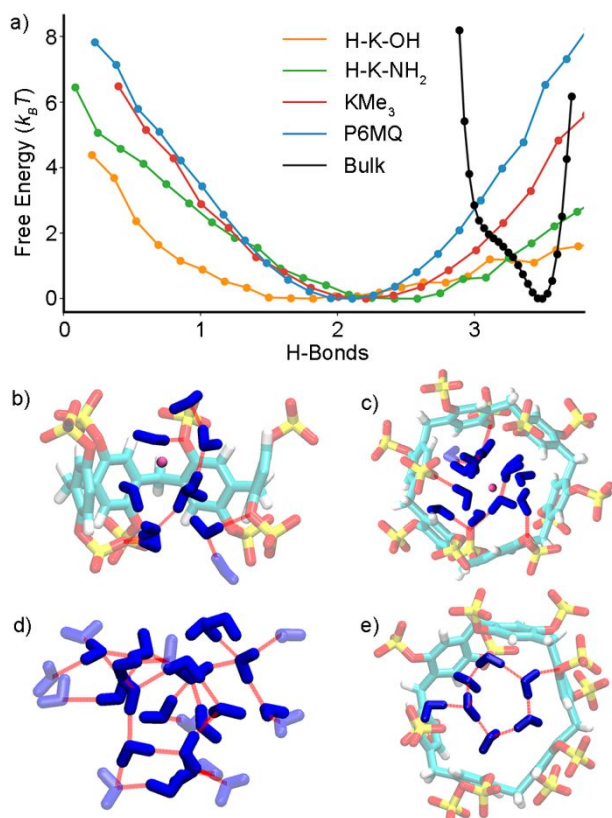water molecules is observed in the MD simulation as shown in Figure 8e.

Figure 8 Characterizing H-bonding in and around P6MQ and complexes. a) Plot of the free energy (see SI for definition) of the system versus average number of hydrogen bonds a water molecule participates in. b,c) The coordination of water molecules by sodium ions in uncomplexed P6MQ, with front side of P6MQ not shown for clarity in panel. Red lines correspond to H-bonds and water molecules are depicted in blue. c. d) An example of the hydrogen bonding network in bulk water. We calculate the hydrogen bonds (red lines) formed within a region of the simulation box defined by $r = 6$ Å, including hydrogen bonds across the surface of the region; solid blue molecules are located within the region and transparent ones are outside. e) Cyclic H-bonded water network observed in the absence of Na$^+$.

We also computed local density plots derived from radial distribution functions which aim to quantify the structure of water around the cavity. Since the radial distribution function $g(r)$ is related to the local density $\rho(r)$ through $\rho(r) = \rho_{bulk} g(r)$, we may directly interpret $g(r)$ as the local density $\rho(r)$.[26] We examined local densities around the P[6]AS sulfate oxygen atoms (4 Å $\leq r \leq$ 7 Å), as presented in Figure 9, and near the P6MQ center of mass ($r \leq$ 4 Å, see Supporting Information). The local density of water molecules for uncomplexed P6MQ shows a broad peak for 2.78 Å < r < 3 Å (considering r ≤ 4 Å waters; O-O distance) (data in Supporting Information) whereas the local density of waters with 4 Å ≤ r ≤ 6 Å shows a sharper peak at 2.80 Å. In contrast, bulk water shows a sharp peak at 2.78 Å. The broad peak seen for P6MQ (r ≤ 4 Å) is consistent with the fact that fewer hydrogen bonds are formed in the core of P6MQ as established in Figure 8c,d. When Na$^+$ is present in the P6MQ cavity, water molecules are oriented such that hydrogen bonding is less likely, resulting in a broader distribution of O-O distances.

From the regions of high local density in Figure 9a we identify two populations of water molecules. There are two regions of high local density in Figure 9a. The leftmost peak in local density corresponds to water molecules which are hydrogen bonded to OSO$_3^-$; the integral of this peak suggests that most sulfate oxygens are H-bonded to a water molecule (e.g. Figure 9b). A single water molecule can form either one or two hydrogen bonds to OSO$_3^-$, and the inter-oxygen distance between water and sulfate corresponds to the leftmost (2.78 Å) peak. The integral of the first peak indicates each OSO$_3^-$ group forms 3.51 H-bonds with water molecules on average, suggesting that water molecules sacrifice H-bonds with one another to preferentially form H-bonds with P6MQ.

The results of the local density and hydrogen bonding analysis suggest that the presence of sodium in the core of the binding cavity of P6MQ causes water molecules to reorient such that they are not able to form hydrogen bonds with one another as effectively as in bulk. Similarly, the intense negative charge of the portals of P6MQ causes water molecules to preferentially form hydrogen bonds with OSO$_3$ over other waters. Our findings unequivocally show that water structure plays an important role in the high affinity binding of P6MQ.
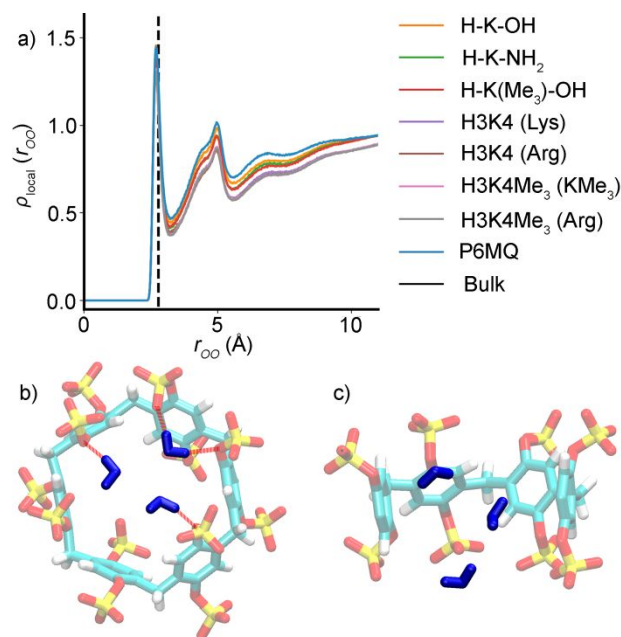

Figure 9 Characterizing the radial location of waters from the center of mass of the OSO$_3^-$ groups. (a) The local density of waters less than 7 Angstroms from P6MQ sulfate oxygens, where the dashes line indicates the local density of bulk water. The local density is averaged over all oxygens. Note that the density of water is largely independent of the bound ligand. (b) The leftmost peak of (a) is explained by water molecules (depicted in blue) that are hydrogen bonded (depicted as red lines) to P6MQ. (c) The broader peak around 5 Å includes water molecules which are not hydrogen bonded to P6A which are typically coordinated by Na+ ions (not pictured, see Figure 8 and Supporting Information).

P6MQ•Amino Acid (Amide) Complexes. Snapshots of a representative geometry of P6MQ•H-HK(Me$_3$)-OH is shown in Figure 10a and snapshots of P6MQ•H-K-OH and P6MQ•H-K-

NH_2 are given in the Supporting Information. We computed the depth of binding (d_{bound}) for these amino acid (amides) by considering the position of the center of mass of each amino acid (amide) relative to P6MQ as described in the Supporting Information. We find that the P6MQ•H-K-OH and P6MQ•H-K-NH_2 complexes show d_{bound} values in the -0.2 to +0.6 Å range which indicates that the α-carbon mainly protrudes (positive d_{bound}) from the P6MQ portal; the ε-carbon sometime protrudes further (negative d_{bound}). The amino acid (amide) NH_3^+ groups form ion-ion / H-bonds to the sulfate groups on P6MQ. In contrast, d_{bound} for P6MQ•H-K(Me$_3$)-OH is +0.4 Å reflecting that the Me_3N^+ group is bound in the center of the P6MQ cavity and the alpha-carbon protrudes from the sulfated portal. These results are in accord with the complexation induced changes in ^{1}H NMR chemical shift discussed above and the geometries depicted in Figures 4b and 10a. In all three cases, the MD simulations show that complex formation results in exclusion of water from the central cavity of P6MQ which constitutes an important driving force for complexation (Figure 8a).
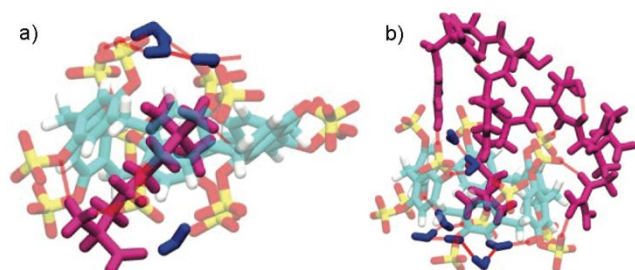

Figure 10 MD simulation structures. a) P6MQ•H-K(Me$_3$)-OH. P6MQ•H-K(Me$_3$)-OH has only one bound conformation; H-K(Me$_3$)-OH is bound at an angle within P6MQ with Me$_3$N+ in the center of the cavity. P6MQ flexes to accommodate the ligand. b) P6MQ•H3K4Me$_3$ (KMe$_3$ bound). P6MQ•H3K4Me$_3$ (KMe$_3$ bound) has a distinct conformation in which the backbone and non-bound sidechains of H3K4Me$_3$ form H-bonds with P6MQ. The H-bonds formed between OSO$_3^-$ and arginine stabilizes arginine within π stacking distance of the P6MQ aromatic walls. In both panels water molecules are depicted in blue, H-bonds as red lines, and the ligand in magenta.

P6MQ•H3 Peptide Complexes. We did not find any differences in the d_{bound} values for P6MQ•H3K4 versus P6MQ•H3K4Me$_3$ when a common residue is bound (e.g. arginine at position 2 or lysine residue at position 4). It appears that secondary interactions between P6MQ and H3 peptide play significant roles in complex geometry. For example, when K or KMe$_3$ at position 4 is bound by P6MQ, we find: 1) that the N-terminus NH_3^+ undergoes backfolding to the sulfate portal to engage in ion-ion / H-bonds, 2) that the arginine at position 2 sometimes engages in π−π stacking interactions (Figure 10b and Supporting Information) with the aromatic wall of P6MQ, and 3) the peptide backbone amide N-H groups form H-bonds to the sulfate groups (Figure 10b). Related H-bonding of peptide N-H groups back to portal C=O groups has been seen with CB[8].[27] These additional modes of interaction that are not available to the amino acids (amides) are likely responsible for the enhanced binding affinities determined for the H3 peptides. And yet the solution-phase preference for binding methylated peptides shown in the ITC data establishes that the engagement of methylated side chains is an important part of recognition in the context of whole peptides.

Conclusions

In summary, we have measured the thermodynamics of binding of P6MQ toward a series of methylated derivatives of the amino acids lysine and arginine by ITC in PBS. We also measure the K_a values for nine amino acid amides to quantify the energetic benefits (costs) of favorable (unfavorable) electrostatic interactions upon complexation. We find a 4.45 kcal mol^{-1} energetic penalty for CO_2^-•••^-O_3SO interactions and a 2.1 kcal mol^{-1} benefit for NH_3^+•••^-O_3SO interactions for P6MQ. The geometry of the complexes were established on the basis of ^{1}H NMR complexation induced changes in chemical shift and by MD simulations. The P6MQ•H-K(Me$_3$)-OH and P6MQ•Asym-H-R(Me$_2$)-OH complexes feature the NMe_3^+ and NMe_2^+ groups located in the center of the P6MQ cavity. Fluorescence competition assays demonstrated that P6MQ recognizes H3K3Me$_3$, H3R2Me$_2$a, and H3R2Me$_2$s with K_d values below 70 nM which is attributed to the presence of secondary ion-ion, π−π, and H-bond interactions of the remainder of the peptide with the portals and outer surface of P6MQ. The MD simulations show that the structure of water in the core cavity of P6MQ and near the sulfated portals are unusual in that a deficiency of H-bonds is observed, in part due to the presence of sodium in the binding cavity. In addition, we find that water molecules preferentially form H-bonds with P6MQ rather than other waters due to the intensely negative charges of the sulfated portals. Overall, the work established P6MQ as a promising new host for the recognition of post-translational modifications in salty media with potential future application as reagents for enzyme assays, analyte detection, and proteomics enrichment strategies.

Experimental.

General Experimental. Chemicals were purchased from commercial suppliers and used without further purification or were prepared by literature procedures.[6, 11l] NMR spectra were measured on commercial instruments operating at 600 MHz for ^{1}H using D$_2$O as solvent. Chemical shifts (δ) are referenced relative to the residual resonances for HOD (4.80 ppm). ITC data were collected on a Malvern Microcal PEAQ-ITC instrument and analyzed using the software provided by the vendor. The fluorescence titrations were performed using a BioTek Cytation-5 multimode plate reader.

Conflicts of interest

Notes and references

1) a) C. D. Gutsche, *Acc. Chem. Res.*, 1983, **16**, 161-170; b) R. A. Rajewski and V. J. Stella, *J. Pharm. Sci.*, 1996, **85**, 1142-1169; c) A. E. Rowan, J. A. A. W. Elemans and R. J. M. Nolte, *Acc. Chem. Res.*, 1999, **32**, 995-1006; d) L. Szente and J. Szejtli, *Adv. Drug Delivery Rev.*, 1999, **36**, 17-28; e) L. Vial, R. F. Ludlow, J. Leclaire, R. Perez-Fernandez and S. Otto, *J. Am. Chem. Soc.*, 2006, **128**, 10253-10257; f) J. Rebek, *Acc. Chem. Res.*, 2009, **42**, 1660-1668; g) F.-G. Klaerner and T. Schrader, *Acc. Chem. Res.*, 2013, **46**, 967-978; h) S. J. Barrow, S. Kasera, M. J. Rowland, J. del Barrio and O. A. Scherman, *Chem Rev*, 2015, **115**, 12320-12406; i) J. H. Jordan and B. C. Gibb, *Chem. Soc. Rev.*, 2015, **44**, 547-585; j) S.-H. Li, H.-Y. Zhang, X. Xu and Y. Liu, *Nat. Commun.*, 2015, **6**, 7590; k) S. Zarra, D. M. Wood, D. A. Roberts and J. R. Nitschke, *Chem. Soc. Rev.*, 2015, **44**, 419-432; l) E. J. Dale, N. A. Vermeulen, M. Juricek, J. C. Barnes, R. M. Young, M. R. Wasielewski and J. F. Stoddart, *Acc. Chem. Res.*, 2016, **49**, 262-273; m) J. Murray, K. Kim, T. Ogoshi, W. Yao and B. C. Gibb, *Chem. Soc. Rev.*, 2017, **46**, 2479-2496; n) J. F. Stoddart, *Angew. Chem. Int. Ed.*, 2017, **56**, 11094-11125; o) Y. Ueda, H. Ito, D. Fujita and M. Fujita, *J. Am. Chem. Soc.*, 2017, **139**, 6090-6093; p) W. Liu, A. Johnson and B. D. Smith, *J. Am. Chem. Soc.*, 2018, **140**, 3361-3370; q) M. Heilmann and K. Tiefenbacher, *Chem. Eur. J.*, 2019, **25**, 12900-12904; r) Y.-M. Zhang, Y.-H. Liu and Y. Liu, *Adv. Mater.*, 2020, **32**, 1806158.

2) M. A. Beatty and F. Hof, *Chem. Soc. Rev.*, 2021, **50**, 4812-4832.

3) a) M. Xue, Y. Yang, X. Chi, Z. Zhang and F. Huang, *Acc. Chem. Res.*, 2012, **45**, 1294-1308; b) H. Zhang, X. Ma, K. T. Nguyen and Y. Zhao, *ACS Nano*, 2013, **7**, 7853-7863; c) T. Ogoshi, T.-A. Yamagishi and Y. Nakamoto, *Chem. Rev.*, 2016, **116**, 7937-8002; d) C. Sathiyajith, R. R. Shaikh, Q. Han, Y. Zhang, K. Meguellati and Y.-W. Yang, *Chem. Commun.*, 2017, **53**, 677-696; e) J. Zhou, G. Yu and F. Huang, *Chem. Soc. Rev.*, 2017, **46**, 7021-7053; f) W. Feng, M. Jin, K. Yang, Y. Pei and Z. Pei, *Chem. Commun.*, 2018, **54**, 13626-13640; g) K. Jie, Y. Zhou, E. Li and F. Huang, *Acc. Chem. Res.*, 2018, **51**, 2064-2072; h) X. Shu, K. Xu, D. Hou and C. Li, *Isr. J. Chem.*, 2018, **58**, 1194-1204; i) H. Zhang, Z. Liu and Y. Zhao, *Chem. Soc. Rev.*, 2018, **47**, 5491-5528; j) Y. Chang, J.-Y. Chen, J. Yang, T. Lin, L. Zeng, J.-F. Xu, J.-L. Hou and X. Zhang, *ACS Appl. Mater. Interfaces*, 2019, **11**, 38497-38502; k) T. Ogoshi, T. Kakuta and T.-A. Yamagishi, *Angew. Chem., Int. Ed.*, 2019, **58**, 2197-2206; l) N. Song, X.-Y. Lou, L. Ma, H. Gao and Y.-W. Yang, *Theranostics*, 2019, **9**, 3075-3093; m) M.-H. Li, X.-Y. Lou and Y.-W. Yang, *Chem. Commun.*, 2021, **57**, 13429-13447; n) K. Wang, K. Velmurugan, X. Tian, M. Zuo, X.-Y. Hu, M. Jordan Jacobs and L. Wang, *Angew Chem Int Ed Engl*, 2021, **60**, 9205-9214; o) H. Yin, X. Zhang, J. Wei, S. Lu, D. Bardelang and R. Wang, *Theranostics*, 2021, **11**, 1513-1526; p) G. Zhang, B. Hua, A. Dey, M. Ghosh, B. A. Moosa and N. M. Khashab, *Acc. Chem. Res.*, 2021, **54**, 155-168; q) H. Zhu, Q. Li, W. Zhu and F. Huang, *Acc. Mater. Res.*, 2022, **3**, 658-668.

4) a) C. Li, J. Ma, L. Zhao, Y. Zhang, Y. Yu, X. Shu, J. Li and X. Jia, *Chem. Commun.*, 2013, **49**, 1924-1926; b) M. Bojtar, A.

Paudics, D. Hessz, M. Kubinyi and I. Bitter, *RSC Adv.*, 2016, **6**, 86269.

5) a) G. Yu, M. Xue, Z. Zhang, J. Li, C. Han and F. Huang, *J. Am. Chem. Soc.*, 2012, **134**, 13248-13251; b) Z. Li, J. Yang, G. Yu, J. He, Z. Abliz and F. Huang, *Org. Lett.*, 2014, **16**, 2066-2069.

6) W. Xue, P. Y. Zavalij and L. Isaacs, *Angew. Chem., Int. Ed.*, 2020, **59**, 13313-13319.

7) a) M. Lachner and T. Jenuwein, *Curr. Opin. Cell Biol.*, 2002, **14**, 286-298; b) A. J. Bannister and T. Kouzarides, *Cell Res.*, 2011, **21**, 381-395.

8) a) Y. Chervona and M. Costa, *Am. J. Cancer Res.*, 2012, **2**, 589-597; b) P. McAnena, J. A. L. Brown and M. J. Kerin, *Cancers*, 2017, **9**, DOI: 10.3390/cancers9010005.

9) C. C. He, J. Y. Xu, J. L. Zhang, D. Xie, H. Ye, Z. Y. Xiao, M. Y. Cai, K. Xu, Y. J. Zeng, H. G. Li and J. Wang, *Human Pathology*, 2012, **43**, 1425-1435.

10) a) R. J. Sims, K. Nishioka and D. Reinberg, *Trends Genet.*, 2003, **19**, 629-639; b) C. Martin and Y. Zhang, *Nat. Rev. Mol. Cell Biol.*, 2005, **6**, 838-849; c) J. C. Black, C. Van Rechem and J. R. Whetstine, *Mol. Cell*, 2012, **48**, 491-507.

11) a) L. A. Ingerman, M. E. Cuellar and M. L. Waters, *Chem. Commun.*, 2010, **46**, 1839-1841; b) K. D. Daze and F. Hof, *Acc. Chem. Res.*, 2013, **46**, 937-945; c) M. A. Gamal-Eldin and D. H. Macartney, *Org. Biomol. Chem.*, 2013, **11**, 488-495; d) J. E. Beaver and M. L. Waters, *ACS Chem. Biol.*, 2016, **11**, 643-653; e) F. Hof, *Chem. Commun.*, 2016, **52**, 10093-10108; f) Y. Liu, L. Perez, M. Mettry, C. J. Easley, R. J. Hooley and W. W. Zhong, *J. Am. Chem. Soc.*, 2016, **138**, 10746-10749; g) H. Peacock, C. C. Thinnes, A. Kawamura and A. D. Hamilton, *Supramol. Chem.*, 2016, **28**, 575-581; h) R. Pinalli, G. Brancatelli, A. Pedrini, D. Menozzi, D. Hernandez, P. Ballester, S. Geremia and E. Dalcanale, *J. Am. Chem. Soc.*, 2016, **138**, 8569-8580; i) Y. Liu, L. Perez, A. D. Gill, M. Mettry, L. Li, Y. S. Wang, R. J. Hooley and W. W. Zhong, *J. Am. Chem. Soc.*, 2017, **139**, 10964-10967; j) T. Gruber, *ChemBioChem*, 2018, **19**, 2324-2340; k) A. G. Mullins, N. K. Pinkin, J. A. Hardin and M. L. Waters, *Angew. Chem., Int. Ed.*, 2019, **58**, 5282-5285; l) A. Shaurya, G. A. E. Garnett, M. J. Starke, M. C. Grasdal, C. C. Dewar, A. Y. Kliuchynskyi and F. Hof, *Org. Biomol. Chem.*, 2021, **19**, 4691-4696; m) Z. Warmerdam, B. E. Kamba, M. H. Le, T. Schrader, L. Isaacs, P. Bayer and F. Hof, *Chembiochem*, 2022, **23**.

12) a) S. Ganapati and L. Isaacs, *Isr. J. Chem.*, 2018, **58**, 250-263; b) C.-L. Deng, S. L. Murkli and L. D. Isaacs, *Chem. Soc. Rev.*, 2020, **49**, 7516-7532.

13) J. Wang, R. M. Wolf, J. W. Caldwell, P. A. Kollman and D. A. Case, *J. Comput. Chem.*, 2004, **25**, 1157-1174.

14) K. A. Connors, *Binding Constants*, John Wiley & Sons, New York, 1987.

15) a) T. Wiseman, S. Williston, J. F. Brandts and L.-N. Lin, *Anal. Biochem.*, 1989, **179**, 131-137; b) A. Velazquez-Campoy and E. Freire, *Nat. Protocols*, 2006, **1**, 186-191; c) J. Broecker, C. Vargas and S. Keller, *Anal. Biochem.*, 2011, **418**, 307-309.

16) a) F. Diederich, *Angew. Chem. Int. Ed. Engl.*, 1988, **27**, 362-386; b) W. M. Nau, M. Florea and K. I. Assaf, *Isr. J. Chem.*, 2011, **51**, 559-577; c) F. Biedermann, V. D. Uzunova, O. A. Scherman, W. M. Nau and A. De Simone, *J. Am. Chem. Soc.*, 2012, **134**, 15318-15323; d) F. Biedermann, W. M. Nau and H.-J. Schneider, *Angew. Chem. Int. Ed.*, 2014, **53**, 11158-11171; e) E. Persch, O. Dumele and F. Diederich,

Angew. Chem., Int. Ed., 2015, **54**, 3290-3327; f) J. W. Barnett, M. R. Sullivan, J. A. Long, D. Tang, T. Nguyen, D. Ben-Amotz, B. C. Gibb and H. S. Ashbaugh, *Nat. Chem.*, 2020, **12**, 589-594.

17) J. Kapuscinski, *Biotech. Histochem.*, 1995, **70**, 220-233.

18) L. Biczok, V. Wintgens, Z. Miskolczy and M. Megyesi, *Isr. J. Chem.*, 2011, **51**, 625-633.

19) B. T. Nguyen and E. V. Anslyn, *Coord. Chem. Rev.*, 2006, **250**, 3118-3127.

20) Y. Shao, L. F. Molnar, Y. Jung, J. Kussmann, C. Ochsenfeld, S. T. Brown, A. T. Gilbert, L. V. Slipchenko, S. V. Levchenko, D. P. O'Neill, R. A. DiStasio, R. C. Lochan, T. Wang, G. J. Beran, N. A. Besley, J. M. Herbert, C. Y. Lin, T. Van Voorhis, S. H. Chien, A. Sodt, R. P. Steele, V. A. Rassolov, P. E. Maslen, P. P. Korambath, R. D. Adamson, B. Austin, J. Baker, E. F. Byrd, H. Dachsel, R. J. Doerksen, A. Dreuw, B. D. Dunietz, A. D. Dutoi, T. R. Furlani, S. R. Gwaltney, A. Heyden, S. Hirata, C. P. Hsu, G. Kedziora, R. Z. Khalliulin, P. Klunzinger, A. M. Lee, M. S. Lee, W. Liang, I. Lotan, N. Nair, B. Peters, E. I. Proynov, P. A. Pieniazek, Y. M. Rhee, J. Ritchie, E. Rosta, C. D. Sherrill, A. C. Simmonett, J. E. Subotnik, H. L. Woodcock, W. Zhang, A. T. Bell, A. K. Chakraborty, D. M. Chipman, F. J. Keil, A. Warshel, W. J. Hehre, H. F. Schaefer, J. Kong, A. I. Krylov, P. M. Gill and M. Head-Gordon, *Phys. Chem. Chem. Phys.*, 2006, **8**, 3172-3191.

21) A. D. MacKerell Jr, D. Bashford, M. Bellott, R. L. Dunbrack Jr, J. D. Evanseck, M. J. Field, S. Fischer, J. Gao, H. Guo and S. Ha, *J. Phys. Chem. B*, 1998, **102**, 3586-3616.

22) W. G. Hoover, *Phys. Rev. A*, 1985, **31**, 1695.

23) M. Parrinello and A. Rahman, *Phys. Rev. Lett.*, 1980, **45**, 1196.

24) D. Van Der Spoel, E. Lindahl, B. Hess, G. Groenhof, A. E. Mark and H. J. Berendsen, *J. Comput. Chem.*, 2005, **26**, 1701-1718.

25) G. A. Tribello, M. Bonomi, D. Branduardi, C. Camilloni and G. Bussi, *Computer Phys. Commun.*, 2014, **185**, 604-613.

26) D. Chandler, *Mechanics. Oxford University Press, Oxford, UK*, 1987, **5**, 449.

27) L. M. Heitmann, A. B. Taylor, P. J. Hart and A. R. Urbach, *J. Am. Chem. Soc.*, 2006, **128**, 12574-12581.